Materials Characterization 225 (2025) 115180

Contents lists available at ScienceDirect

Materials Characterization

journal homepage: www.elsevier.com/locate/matchar

Reduction of compression-tension yield asymmetry in binary Mg—Gd alloys via mastering their crystallographic textures☆

Dongsheng Han [a], Cai Chen [b,*], Mingchuan Wang [b], Nathalie Siredey-Schwaller [c], Zhonghua Du [a], Sen Yang [d], Fengjian Shi [e], Benoit Beausir [c], Amèvi Tongne [f], Laszlo S. Toth [c,g]

[a] Nanjing University of Science and Technology, Xiaolingwei 200, Nanjing 210094, PR China
[b] Sino-French Engineer School, Nanjing University of Science and Technology, Xiaolingwei 200, Nanjing 210094, PR China
[c] Laboratoire d'Etude des Microstructures et de Mécanique des Matériaux (LEM3), Université de Lorraine, CNRS, Arts et Métiers ParisTech, F-57045 Metz, France
[d] School of Materials Science and Engineering, Nanjing University of Science and Technology, Xiaolingwei 200, Nanjing 210094, PR China
[e] School of Materials Science and Engineering, Jiangsu University of Science and Technology, Zhenjiang 212003, PR China
[f] Laboratoire Génie de Production, Université de Technologie Tarbes Occitanie Pyrénées, Université de Toulouse, 65000 Tarbes, France
[g] Metal-forming and Nanotechnology, Institute of Physical Metallurgy, University of Miskolc, 3515 Miskolc, Hungary

A R T I C L E I N F O

Keywords:
Mg—Gd alloy
Double ECAP
Compression-tension yield asymmetry (CTA)
Crystallographic texture
Polycrystal plasticity simulation

A B S T R A C T

Compression-tension asymmetry (CTA) in yield strength is one of the issues that hinders widespread application of wrought Magnesium (Mg) alloys. Strong basal texture formed in thermomechanical processing and the difference in activation of deformation twinning in tension and compression are responsible for CTA. To reduce CTA, the readily implementable Double Equal Channel Angular Pressing (D-ECAP) is used in this study for altering the microstructure and texture of Mg samples. Mg bars containing 1, 5, and 10 wt% Gd were subjected to D-ECAP at 400 °C. Due to plastic strain, the average grain sizes decreased from several hundred microns to about 13.4 μm, 5.6 μm, and 5.1 μm, respectively. All processed samples showed high strength and characteristics shear textures. The crystallographic textures displayed the so-called C1-C2 and B fibers. C1-C2 were the major fibers in the 1 % and 5 % Gd samples, while the B and C1 fibers appeared in the 10 % Gd sample. C1-C2 requires high activity of pyramidal $<c + a>$ slip, and B belongs to basal slip. The CTA was measured by the ratio of the compression/tensile yield stress and significant increase in CTA was obtained on the D-ECAP processed samples with respect to the base alloys. The CTA reached 0.85 in the Mg—10Gd alloy without sacrificing the yield strength. Polycrystal plasticity simulations were done using the experimental textures and good reproduction of the CTA values were achieved. The simulation results also revealed the relative activity of the slip and twinning systems for understanding the mechanisms that control the CTA. The results of this study revealed that D-ECAP is an efficient processing technology that can be widely used in the preparation of high-performance Mg—Gd alloys.

1. Introduction

Magnesium (Mg) alloys are attractive structural metallic materials due to their low density, about 1/3 Fe and 2/3 Al. They are widely applied in transportation, aerospace industry, and consumer electronics, etc. [1–4]. However, most Mg alloys have an HCP crystalline structure, which has lower symmetry compared to cubic structured metals. Therefore, a Mg alloy has poor plasticity under room temperature deformation conditions [5]. To produce Mg with better mechanical properties, a thermomechanical process, such as extrusion or rolling, is demanded to get fine microstructures and fine secondary phase particles [5,6]. Unfortunately, strong basal textures, such as ⟨0001⟩ perpendicular to the extrusion direction (ED) in extrusion, or parallel to the normal direction (ND) in rolling, are produced, leading to poor mechanical performance, like mechanical anisotropy , and compression-tension yield asymmetry (CTA) in a Mg alloy. In most cases of wrought Mg alloy with strong basal texture, the compression yield strength (CYS) is smaller than the tensile yield strength (TYS) [,8]. The CTA value is commonly defined as the ratio of the compression yield strength to the tensile one: CTA = CYS/TYS. In some cases, the CTA is

☆ This article is part of a Special issue entitled: 'ICOTOM' published in Materials Characterization.

* Corresponding author.
E-mail address: cai.chen@njust.edu.cn (C. Chen).

https://doi.org/10.1016/j.matchar.2025.115180
Received 22 November 2024; Received in revised form 28 April 2025; Accepted 17 May 2025
Available online 19 May 2025

only 0.5 [8], which results in limited formability and restricts the industrial applications of Mg alloys.

The study of formation mechanism and optimizing strategies of the CTA in wrought Mg alloys has been the focus issue in research in the past decade [8–11]. Reports [10–12] reveal that the different plastic deformation mechanisms under tension and compression are the main reasons for CTA in Mg alloy, especially the extension twinning. For example, during compression in the ED direction of an extruded Mg bar, a grain oriented with its c-axis perpendicular to ED is stretched, so {10−12} type extension twin (ET) can be readily activated because it has a lower critical resolved shear stress (CRSS, 2.0–2.8 MPa [13]). However, if the loading is inverted, that is tension is applied, the same ET cannot be active because twinning can take place only in one direction (the twinning direction). Therefore, other deformation mechanisms, such as pyramidal slip, are needed which have much higher CRSS than ET, leading to a CTA value less than 1.0. Therefore, alteration of twinning activation becomes an important method to reduce the CTA of Mg alloy, either eliminating the generation of twins or making the twinning activation more consistent when the material is loaded in different directions. In wrought Mg, the ability of twinning activation is strongly related to the grain size [14–16], alloying elements [17,18] and crystallographic texture [17,19]. To eliminate twinning, it can be done by reducing drastically the grain size [20]. Studies reveal [14,15] that deformation twin is inhibited when the grain size is less than 3 μm, which can affect CTA. Yin et al. [20] reports that the critical grain size for reducing twinning is about 0.8 μm. However, wrought Mg alloys are generally produced in high temperature (about 250 °C ~ 450 °C), it is difficult to refine the grain size of Mg alloys to less than 1 μm [21–23]. Therefore, while using thermomechanical process to refine the grains, altering the texture deserves special attention for twinning activation.

Alloying with rare earth (RE) elements is considered to be an efficient method to reduce the basal texture of Mg alloys and promoting the grain refinement [24,25]. By the addition of Gd or/and Y in Mg, a so-called "RE" texture component can be produced instead of a basal texture [26–28]. These RE elements can form precipitates to promote dynamic recrystallization through the particle-stimulated nucleation (PSN) mechanism [29], and inhibit grain growth through the dragging effect of solution RE atoms [30], so to achieve grain size refinement of Mg alloys. The basal texture weakening is due to oriented nucleation at shear bands and PSN during dynamic recrystallization (DRX) [31]. Researches suggested that {10–12} ET can be suppressed in Mg alloy with high content Gd addition and the appearance of RE texture will help adjusting the twinning activation [32–34]. Consequently, isotropic mechanical properties are expected to be achieved in Mg—Gd based alloys. However, in practice, due to the limited texture weakening that can be achieved by adding rare earth elements alone and the inhomogeneous microstructure with relatively large (>5 μm) grain size, CTA is still an annoying problem in Mg—Gd based alloys produced by traditional thermomechanical processes (extrusion & rolling) [35–37].

Equal channel angular pressing (ECAP) is an efficient method to achieve grain refinement and texture control in bulk Mg alloy,as the sample size of Mg alloy that can be processed by ECAP has researched 50 mm × 50 mm × 100 mm [38–40], which is considered a promising technique for industrial application. After six ECAP passes, the grain size in a Mg alloy can be reduced to about 1 μm [41]. Furthermore, the ECAP process can also alter the basal texture to improve the ductility of Mg alloys. The texture evolution of ECAP-deformed Mg alloys in different processing routes has been well understood [42–46]. In Mg alloy processed by ECAP with die angle of 90°, texture components [47] with basal plane || shear plane (B fiber), <a > || shear direction (P fiber), c-axis rotated towards the shear plane by 30° (Y fiber), and c-axis rotated 90° in the shear direction then ±30° in the shear plane direction(C1/C2 fiber) are potential components. Applying ECAP to produce Mg-RE alloys, more texture components and a more uniform microstructure are possible for reducing the CTA. Comparing to other processing routes, the first two ECAP deformation passes in route C are considered to be a more effective process for grain refinement and texture modification [43–45]. For route C [48], the sample is rotated by 180° along the normal direction between ECAP passes; the shear planes of each pass are coincident and the shear direction of the two adjacent deformation passes is opposite. Instead of six subsequent ECAP passes, it is desirable to achieve the necessary grain refinement and texture modification of Mg—Gd based alloys in a single step, which is possible by connecting two ECAP processes in a single die.

In this study, a novel die; the D-ECAP (double equal channel angular pressing) is proposed which can readily achieve two ECAP passes in a single step; in route C. Mg—Gd alloys with various Gd contents were submitted to D-ECAP process. The microstructure and texture of D-ECAP processed Mg—Gd binary alloys were quantitively examined by optical micrographs (OM), scanning electronic micrographs (SEM), X-ray diffraction (XRD) and electron back-scattering diffraction (EBSD). The asymmetric mechanical response and the corresponding deformation mechanisms under uniaxial tension and compression at room temperature are discussed in detail. Particularly, the CTA of the D-ECAP processed samples was successfully reproduced by polycrystal modeling. The results of this study provide insights into the microstructure refinement, texture optimization, and the asymmetric mechanical response of Mg—Gd alloys.

2. Experimental

Binary Mg—Gd alloys with Gd addition of 1, 5 and 10 wt% were used for D-ECAP deformation in this study. For preparing the raw Mg-x%Gd ingots, pure Mg (>99.7 wt%) and Mg—30Gd (wt%) master alloys were used. The raw materials were melted in an electric resistance furnace under a mixed gas atmosphere of SF_6 and CO_2 at about 730 °C. After refining and removing impurities, the molten material was poured into the casting mold, which had a diameter of 60 mm and a length of 300 mm. The chemical compositions of the obtained alloys were determined by using an inductively coupled plasma spectrometer analyzer. The exact Gd contents were 0.91, 5.49 and 9.57 wt%, respectively. Samples were cut out from the ingot by electric spark wire to a cylindrical shape with a diameter of 20 mm and length of 36 mm. Fig. 1a shows the thermomechanical process applied to the samples. First a homogenization heat treatment was carried out at 530 °C for 10 h, followed by quenching into warm water (~60 °C). The samples were pre-heated at 400 °C for 20 min prior to D-ECAP, also the die was heated to 400 °C, then D-ECAP was carried out at an extrusion speed of 22 mm/s (see the schematic of D-ECAP in Fig. 1b). The intersection angle of the double channel was 105°, with outer corner angles of 75°. D-ECAP with 105° channels can achieve two ECAP passes in route C in a single step, with a total von-Mises equivalent strain of 1.15 [49].

For the analysis of the microstructures and the crystallographic textures, samples were cut from the center part of the processed rods in longitudinal section with their studied surfaces containing the extrusion (ED) and normal (ND) directions. The specimens were mechanically polished, followed by argon-ion etching. The microstructures were characterized by an optical microscope (OM, Axio Vert.A1) and by the

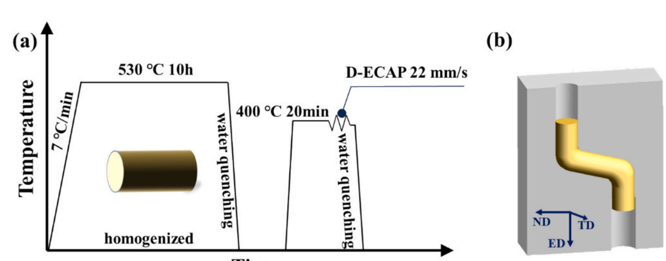

Fig. 1. Schematic of the thermo-mechanical process (a), and the D-ECAP module (b).

electron backscattered diffraction (EBSD) technique. EBSD measurements were done at 15 kV, with a step size of 0.4 μm, using a ZEISS Ultra Plus scanning electron microscope (SEM) equipped with an EBSD camera and the AZtec software package (Oxford Instruments). The morphology, distribution and chemical composition of second phase particles were examined by a scanning electron microscope (SEM) equipped with an energy dispersive X-ray spectrometer (EDS) at 15 kV and transmission electron microscopy (TEM, FEI Tecnai 20), using the standards of pure Mg and Gd. Dog-bone shaped samples (gauge size of 2 mm × 3 mm × 5 mm) were machined for uniaxial tensile test and cylindrical samples (diameter and length of 6 × 6 mm) were prepared for compression tests. Both tensile test and compression tests were performed along ED under a strain rate of $1.5 \times 10^{-3}\ s^{-1}$.

3. Experimental results

3.1. Microstructure evolution

The optical microscopy (OM) images and related grain size distributions of the D-ECAP processed Mg-xGd alloys are shown in Fig. 2. It can be seen that the microstructure characteristics varied by the Gd content. After plastic deformation, the Mg—1Gd alloy displayed relatively larger grain size and the occurrence of dynamic recrystallization (DRX), while there were also some areas where DRX did not take place. It is notable that numerous twins were formed and maintained during the deformation. In the OM images, the number of twin-boundaries was decreased with increasing Gd content, and finally not visible in the OM images of the Mg—10Gd alloy. Grain size distributions were computed by using the mean diameter measurement in Image Pro Plus software, three maps were considered for each sample (more than 4000 grains) to obtain good statistics. Prior to performing the calculations, image processing software was used to identify grain boundaries and particles in OM images. White color was used for the grain interiors and black for the grain boundaries (Fig. 2d, e, f). This enabled the Image Pro Plus software to distinguish between grains and grain boundaries based on color contrast. In addition, the small number (less than 10 grains had obvious twinning among thousands of grains) of abnormal twins that appeared in the Mg—1Gd and Mg—5Gd samples were not accounted. The results show that the average grain size decreased remarkably from ~13.4 μm to ~5.6 μm when the Gd content increased from 1 wt% to 5 wt %, and the distributions became narrower. The Mg—10Gd alloy only had a slightly lower average grain size (about 5.1 μm) compared to Mg—5Gd alloy. According to several reports [24,50,51], an increasing Gd content (Gd content <5 wt%) in Mg alloys promotes dynamic recrystallization by grain boundary segregation to achieve a homogenous microstructure distribution with lower average grain size. However, when Gd addition is more than 5 wt%, Gu et al. [52] and Lee et al. [53] found that further grain refinement in high Gd contented Mg alloy is limited, so that the grain size of extruded Mg—15Gd or Mg—10Gd alloy is about 1 μm less than extruded Mg—5Gd. The reason for this phenomenon is that Gd precipitates in large quantities in the form of micron-sized particles.

In addition to grain size refinement, precipitation is another important strengthening mechanism in Mg-RE alloys, especially for Mg—Gd based alloys, due to the significant differences in solid solubility between high temperature and room temperature. Optically, in our experiments, Gd-enriched fine particles appeared in the samples as black dots with irregular shapes after processed by ECAP. However, they were too small for precise analysis by OM, so SEM was used for further investigation of the second phase; the morphologies are presented in Fig. 3.

Comparing to traditional extrusion processes, shear deformation induced by ECAP is more favorable for producing uniform particle dispersion, instead of forming fibrous structures [54,55]. As can be seen in Fig. 3a-c, the second phases particles show a nearly random distribution in all deformed samples. From the local magnification image in Fig. 3d-f, some more details can be revealed. In Mg—1Gd, some fine particles grouped together in clusters, and some other particles exhibited cuboidal shapes and larger size. By adding more Gd to Mg, the clusters disappeared and more cuboidal shaped particles were obtained, especially at grain boundaries, as shown in Fig. 3f. Fig. 3g-i shows the statistics of the particle sizes in different samples (using Image Pro Plus software), with around 300 particles (minimum size about 200 nm) counted for each sample. The average particle sizes of the three alloys were ~ 1.15 μm, ~1.47 μm, and ~ 1.71 μm, and their relative area fractions were ~ 0.27 %, ~0.48 % and ~ 0.54 % in the 1, 5, and 10 % Gd compositions, respectively. Both the average particle size and area fraction were increased with increasing Gd content. It can be also found

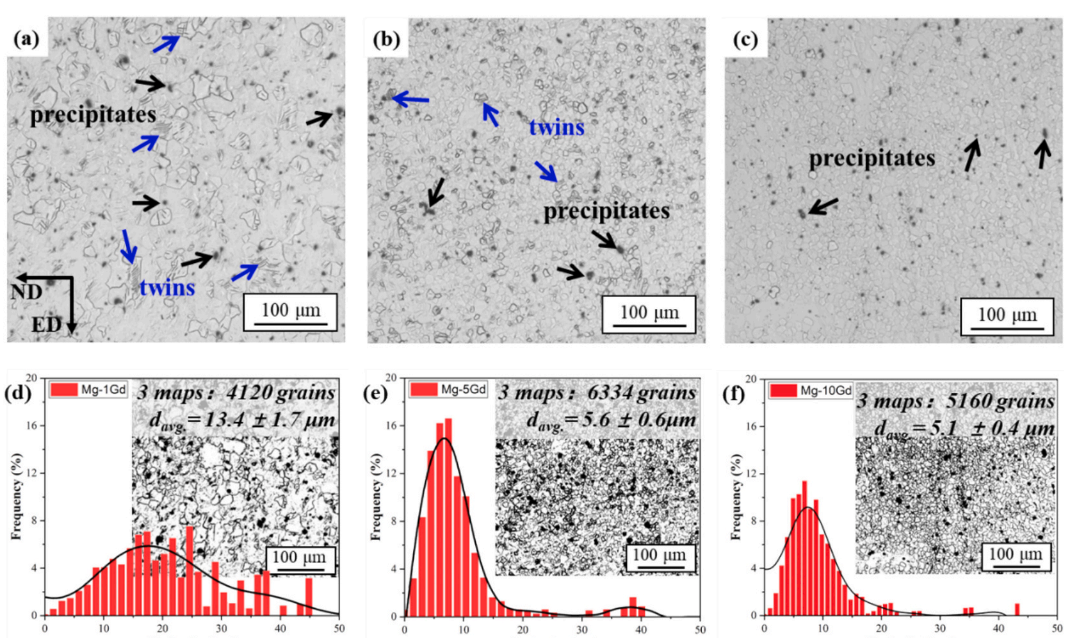

Fig. 2. Optical micrographs of D-ECAP processed samples and corresponding area fraction grain size distributions in D-ECAP processed samples: (a, d) Mg-1Gd; (b, e) Mg-5Gd; (c, f) Mg—10Gd.

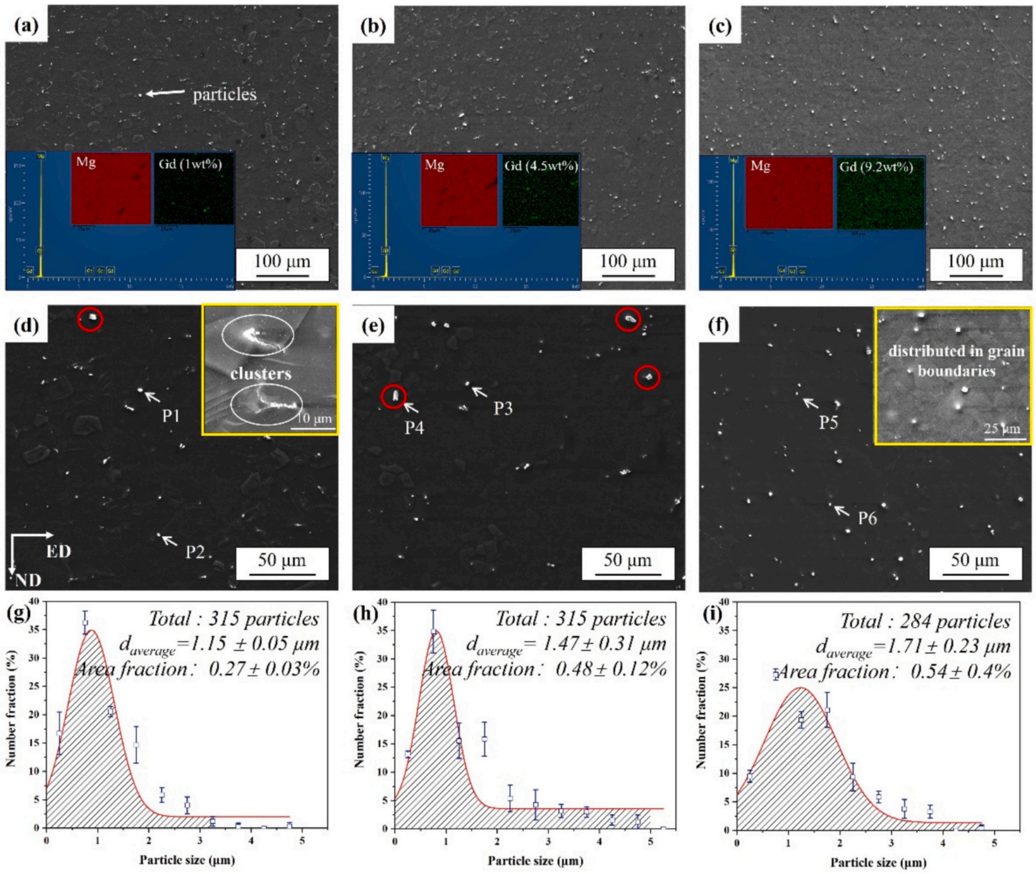

Fig. 3. SEM morphologies of D-ECAP processed samples: (a,d) Mg-1Gd; (b,e) Mg-5Gd; (c,f) Mg—10Gd. The particle size statistic corresponding to the SEM images: (g) Mg-1Gd; (h) Mg-5Gd; (i) Mg—10Gd.

from the fitted Gaussian lines in Fig. 3 that the size differences of the particles diminished. Fig. 4 shows the particle distribution characterized by TEM, in order to compare the size of the nano-particles, a white square (200 nm × 200 nm) is placed in each image. The results show that with increasing Gd addition, Gd elements prefer to form larger particles around grain boundaries and nano-particles with size below 200 nm are rarely observed in those three samples.

The possible phases of the particles were identified by EDS analysis and the results are summarized in Table 1. Although the particles had small sizes, which interfere with quantitative chemical analysis, the chemical results led us to conclude that the particles were Mg_5Gd phases, which is a well-known stable second phase in Mg—Gd alloys [56]. Several particles appeared in abnormal large size with irregular shapes, and were rich in Gd content.

The EBSD inverse pole figure (IPF) maps acquired on the ED-ND plane of the processed samples are shown in Fig. 5a-c. The ED axis of the sample coordinate system was used for identification of the orientation by colors shown in the unit triangle. All maps show a not completely recrystallized microstructure with some coarse grains elongated along the shear direction. The disorientation distributions of the

Table 1
EDS analysis of the particles in Fig. 3.

Sample	Position	Mg content (at.%)	Gd content (at. %)	Possible Phase	Size (μm)
Mg-1Gd	P1	83.4	16.6	Mg_5Gd	1.8
	P2	82.2	17.8	Mg_5Gd	1.6
Mg-5Gd	P3	80.7	19.3	Mg_5Gd	1.6
	P4	47.9	52.1	Rich-Gd particle	2.8
Mg-10Gd	P5	86.6	12.4	Mg_5Gd	1.2
	P6	83.7	16.3	Mg_5Gd	1.3

three deformed samples are shown in Fig. 5d-f, where the low angle grain boundaries (LAGBs, <15°) were calculated as 8.26 %, 3.01 % and 4.46 %. The disorientation distributions show a tendency to adopt the random Mackenzie distribution [57,58] with increasing Gd contents.

In this work, grains with an average intragranular disorientation below 3° were considered as dynamically recrystallized (DRX) grains. The area fractions of DRX (f_{DRX}) grains were determined in Fig. 5g-i. They were 68.77 %, 86.64 %, and 89.41 % in the Mg—1Gd, Mg—5Gd,

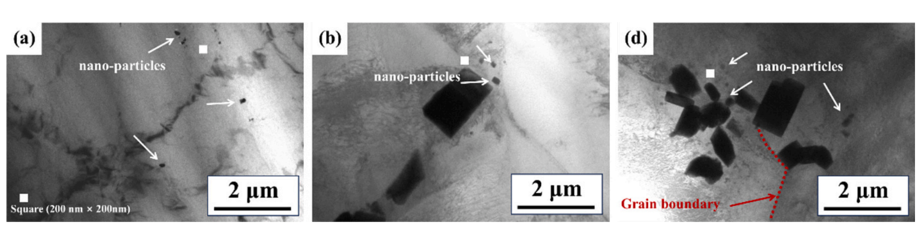

Fig. 4. Particles characterization by TEM: (a) Mg-1Gd; (b) Mg-5Gd; (c) Mg—10Gd.

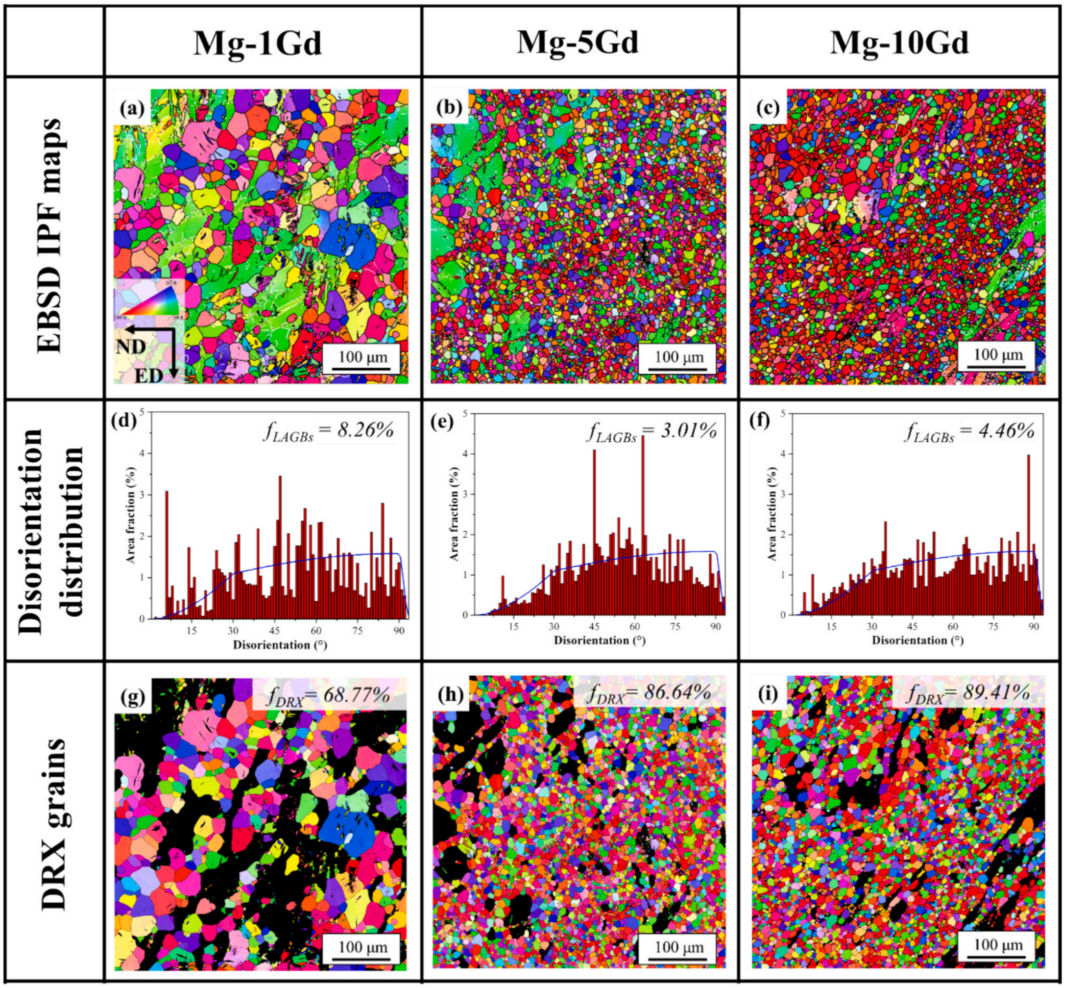

Fig. 5. EBSD results in inverse pole figures (IPFs) with next-neighbor disorientation distributions: (a) Mg—1Gd, (b) Mg—5Gd, (c) Mg-10Gd; In (d-f) histograms of the disorientation distribution, the random Mackenzie distribution is in blue line, and (g-i): IPF maps of DRX grains. Black regions in (g-i) are not recrystallized. (For interpretation of the references to color in this figure legend, the reader is referred to the web version of this article.)

and Mg—10Gd samples, respectively. Therefore, it is demonstrated here that Gd alloying is significantly promoting the dynamic recrystallization in Mg.

3.2. Texture results

In order to obtain sufficient statistics, more than 2000 grains were analyzed for texture calculations from the EBSD images. The textures of various Gd content D-ECAP-deformed samples are presented in Fig. 6 in {0001} and {10−10} poles figures. The key-figures of the expected ideal orientations are also presented in Fig. 6d [47] for the two kinds of pole figures, rotated into the position of the theoretical shear plane of the process. As can be seen, the measured texture components can be identified with the ideal orientations of HCP shear textures shown in the key figures, which is expected, because the D-ECAP process is imposing essentially simple shear to the samples. One can notice remarkable differences in the textures as a function of Gd content. At 1 % and 5 % Gd, the main texture components were the C1 and C2 components, although they are rotated in in clockwise direction, roughly about by 15°, with respect to the ideal ones. On the contrary, the texture at 10 %, Gd differed considerably: the C2 component nearly vanished and a new component appeared, the B, together with the C1. As the change in the texture is substantial at high Gd content, there must be differences in the operating deformation mechanisms, which will be discussed in the Discussion part.

3.3. Mechanical behaviors

The engineering strain-stress curves of tensile and compression tests are presented in Fig. 7a-b and the mechanical properties of ultimate tensile strength (UTS), tensile yield strength (TYS), tensile elongation to failure (TEL), ultimate compression strength (UCS), compression yield strength (CYS) and compression strain until fracture (CEL) are listed in Table 2. For the homogenized samples, the TYS and UTS increased with Gd content, while TEL decreased. CEL shows irregular variations. In solid solution treatment of Mg—Gd binary alloy, coarse grain size, impurity particles and Gd-rich particle are reported to be not fully eliminated by heat treatment [59,60]. Therefore, the limited strength and varying CEL of the homogenized alloy are concluded to be attributed to those casting defects. After D-ECAP process, the tensile strength and TEL were simultaneously improved. The Mg—1Gd sample exhibited the best TEL of ~41 % while the TYS and UTS were the lowest. With the highest Gd addition, the TYS of Mg—10Gd sample increased 54 % and the TEL decreased 27.7 % compared to the Mg—1Gd. On the contrary, the results of compression tests showed an opposite trend in the CEL, where Mg—10Gd presented the best CYS and CEL.

The yield asymmetry in compression yield stress / tensile yield stress (CYS/TYS) are presented in Fig. 7c. In common sense, the yield asymmetry is better when the value of CYS/TYS is closer to 1. Therefore, the results show that the yield asymmetry of Mg—Gd binary alloy can be improved byD-ECAP process.

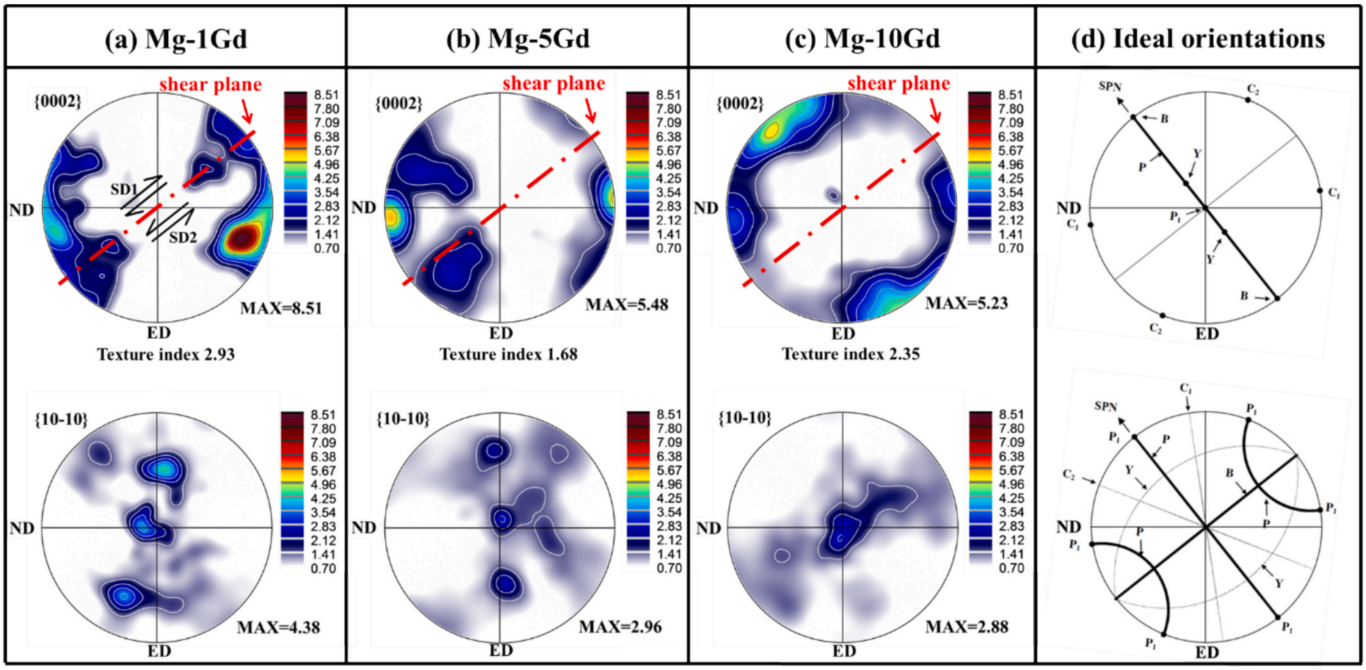

Fig. 6. {0002} and {10−10) pole figures of the textures based on EBSD measurements: (a) Mg-1Gd; (b) Mg-5Gd; (c) Mg—10Gd. The key pole figures for the ideal orientation positions are also presented in (d) [47].

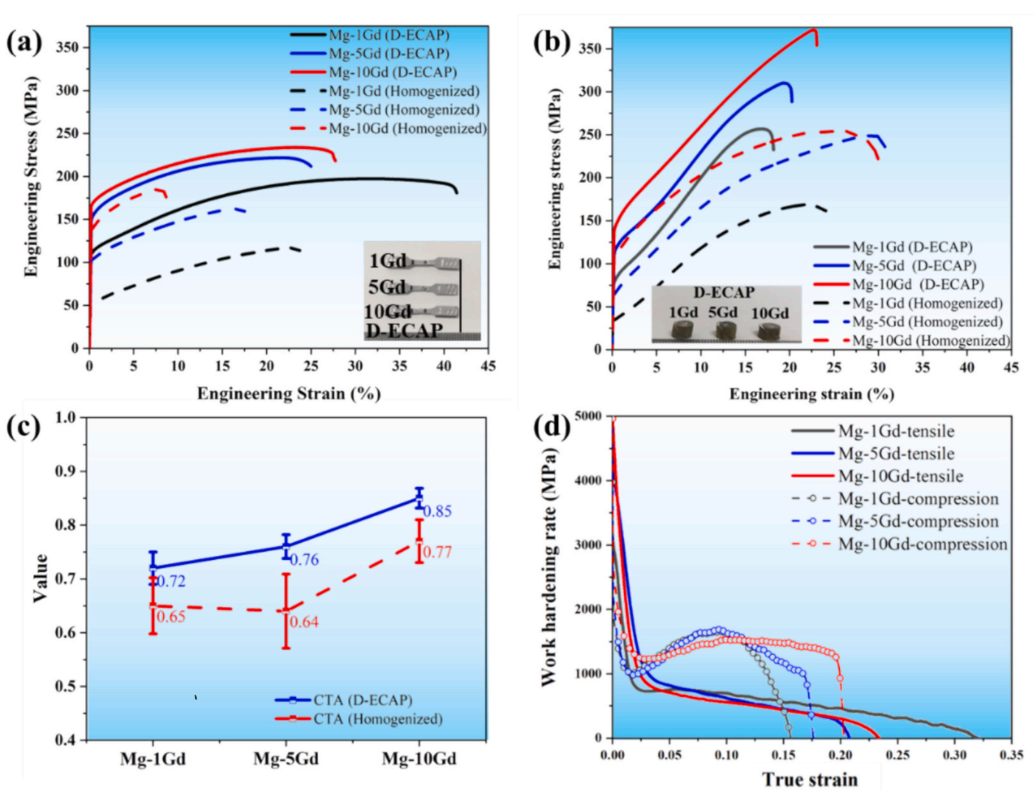

Fig. 7. Mechanical properties at room temperature: (a) engineering tensile strain-stress curves; (b) engineering compression strain-stress curves; (c) yield asymmetry in compression yield stress / tensile yield stress (CTA); (d) work hardening rate of D-ECAP processed samples.

Fig. 7d presents the variation of the work hardening rate with true strain of the processed samples, calculated from tensile and compression curves. During compression tests, all samples showed an intermediate increase in strain hardening between yield and fracture. In general, strain hardening is higher during compression compared to tension, which indicates that deformation twins influenced the strain hardening behavior more in compression.

Table 2
Mechanical properties measured in tensile and compression testings.

Sample	Process	Test	Yield stress [MPa]	Ultimate stress [MPa]	Elongation to failure [%]	CTA (CYS/TYS)
Mg-1Gd	Homogenized	Tensile	50.49	117.05	24.05	0.65
		Compression	32.92	168.48	24.51	
	D-ECAP	Tensile	112.04	197.28	41.03	0.72
		Compression	81.36	256.63	17.87	
Mg-5Gd	Homogenized	Tensile	103.87	162.19	17.53	0.64
		Compression	66.34	248.96	30.39	
	D-ECAP	Tensile	154.82	221.63	24.55	0.76
		Compression	117.95	309.88	19.84	
Mg-10Gd	Homogenized	Tensile	138.72	184.72	8.23	0.77
		Compression	106.54	254.82	29.51	
	D-ECAP	Tensile	173.01	233.73	27.12	0.85
		Compression	146.62	317.69	22.57	

3.4. Fracture morphology under tension

After tensile testing, SEM was used to characterize the fractured samples on the ED-ND and ND-TD planes. As can be seen from the results of the ED-ND side views in Fig. 8a,c,e, the microstructure of samples with different Gd contents changed differently after stretching. In the Mg—1Gd sample, the grains were significantly elongated along the deformation direction (ED). Microcracks were visible at the grain boundaries with rich RE element segregations or near to large precipitates. This phenomenon was similar in the Mg—5Gd sample (Fig. 8c). However, due to the larger Gd content, the ductility of the Mg—5Gd and Mg—10Gd samples decreased by more than 10 %. In addition, more Gd content introduced more second-phase particles, including cuboidal shaped and fine precipitate particles as shown in Fig. 8e. It can be clearly seen from the fractured microstructure of the Mg—10Gd samples that some cuboidal shaped particles fractured during the tensile test and several micro-voids were formed around large particles. Furthermore, it is worth mentioning that deformation twins were present in all ND-ED surfaces of the fractured samples.

The morphology of the fracture is a visual representation of the fracture behavior, which can directly reflect the characteristics of brittle or ductile fracture. Fig. 8b, d and f present the fracture surface and locally amplified images of Mg—Gd samples after tensile test. Fig. 8a shows that the Mg—1Gd sample had ductile fracture, a large number of fine dimples and a few cleavage planes (<10 %) contributed to the morphology. These cleavage planes are related to the inhomogeneous

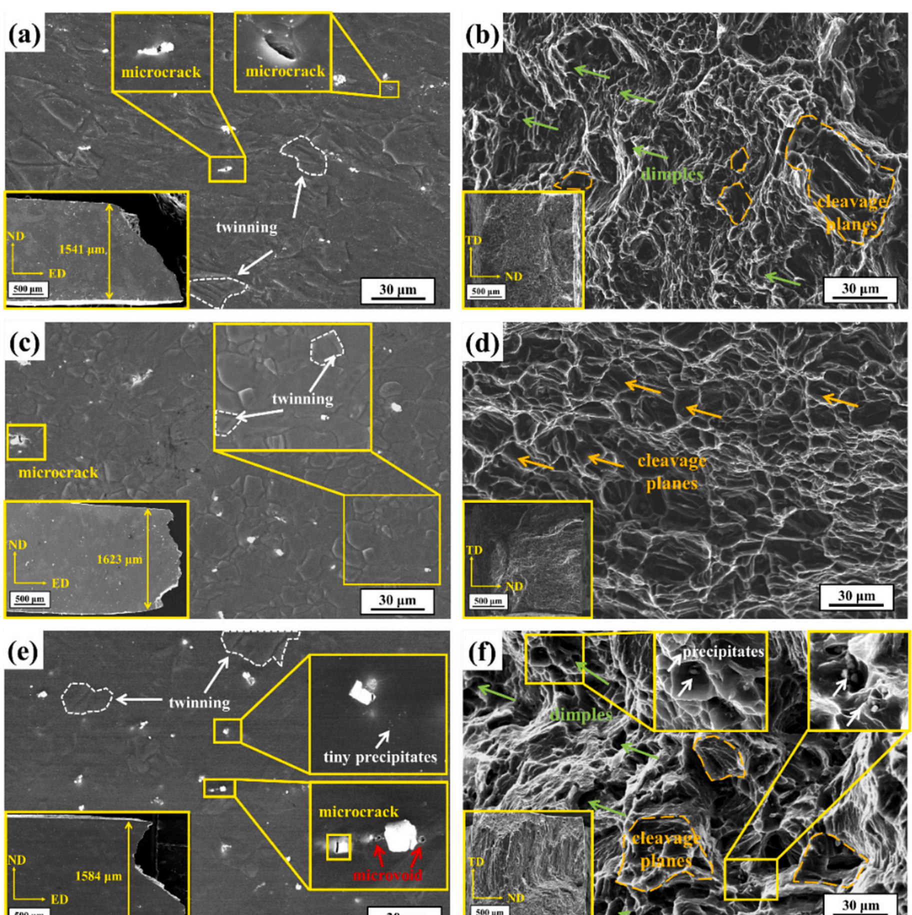

Fig. 8. Microstructure of fractured samples in the ED-ND planes and fractured mophology in ND-TD plane: (a-b) Mg-1Gd; (c-d) Mg-5Gd; (e-f) 10Gd.

deformation of the sample. In the Mg—5Gd sample, the cleavage planes became the dominant fracture feature, and no obvious dimples were observed in Fig. 8d. According to the mechanical properties in Fig. 7a, it can be seen that the elongation to failure of the Mg—10Gd sample is between that of the Mg—1Gd and Mg—5Gd. The fracture behavior of the Mg—10Gd sample became more complex as shown in Fig. 8f, both brittle fracture and ductile fracture regions evidently existed, and precipitates were found in the core of some dimples.

4. Discussion

4.1. Microstructure

In order to better understand the evolution of the microstructures during the ECAP process, an investigation was conducted on the non-dynamically recrystallized (no-DRX) grains. They were selected from Fig. 5a-c with the criterion of more than 3° grain orientation spread (GOS), and reproduced in Fig. 9a-c. Some individual grains were selected and accumulative disorientation angles were measured inside these grains. As shown in Fig. 9g-i for grains L1-L6, the disorientation angles can be quite high. There are sudden disorientation increases at sub-grain boundaries, see for example L1'and L4. Such features are typical for the occurrence of continuous DRX which is producing increasing lattice curvature leading to grain refinement.

It can be clearly observed in Fig. 9, that almost all no-DRX grains are aligned with their major axis nearly parallel to the shear plane in our D-ECAP setup. It is also evident, that all these grains are relatively large grains; much larger than the average grain size. However, their elongated shapes in the direction of the shear are unexpected, because the initial grain shapes were not elongated. Indeed, during D-ECAP, the shear direction is inverted in the second stage of the extrusion, so the initial non-elongated grain shape should be fully recovered. Such grain shape recovery was documented in Route C ECAP [61], and quite obvious. However, of DRX took place during D-ECAP, and dislocation slip is not fully reversible in Mg due to the microstructure [62,63]. These two effects make the grain shape hard to be recovered. Moreover, extension twins appeared during the first D-ECAP stage. Fig. 10 shows the geometry and the stress state schematically. Adopting the simple shear model of ECAP, the theoretical shear plane is at 52.5° orientation with respect to the vertical direction in Fig. 10. The shear stress state acting parallel to the shear plane can be split into compression and tension stress components, which are at 45° oriented with respect to the shear. It is well-known that the highest occurrence of extension twins is expected inside grains that have their c-axis parallel to the extension stress state. Then the twinning plane of the most active variant of extension twins is oriented nearly parallel to the shear plane of the process, the difference is only 2°, see in Fig. 10. Therefore, the orientation of the twin interfaces should be at 50.5° with respect to the

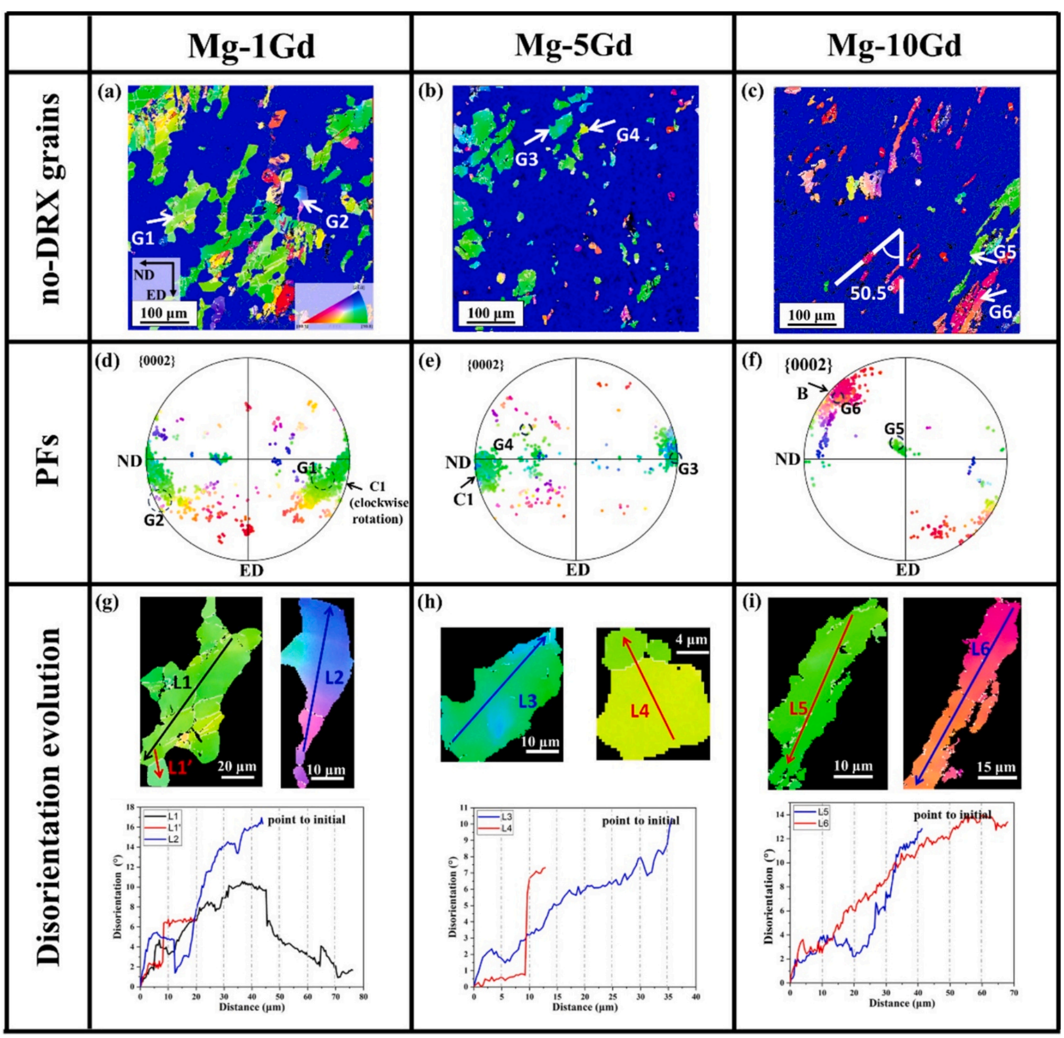

Fig. 9. Dynamic recrystallization analysis: (a-c) no-DRX grains (GOS > 3°) with their {0002} PFs represented by the same colors of the grains in (d-f). In blue regions the GOS is less than 3° (black regions had no diffraction patterns). (g-i): IPF maps of six selected grains and disorientation evolution on their diagonal lines from the initial point. (For interpretation of the references to color in this figure legend, the reader is referred to the web version of this article.)

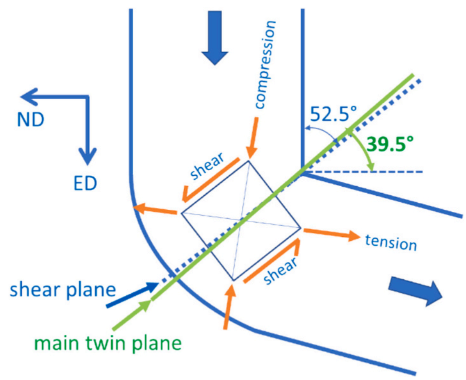

Fig. 10. Schematic figure for showing the stress/strain state during ECAP with 105° channels.

vertical direction. This theoretical orientation agrees well with the orientations of the large axes of the elongated grains experimentally observed and presented in Fig. 8c. Of course, deviations are allowed, because extension twins can also be activated when the grain is not exactly in the best ideal position with respect to the maximum tensile stress direction. These elongated grains can be original matrix grains, or they can be extension twins as well. In each case, they are initially limited between two extension twin interfaces. These interfaces can become wavy during the crossing into the die, due to locally developing strain gradients and DRX-induced bulging of the boundaries. According to the color code in Fig. 9a, they can be identified in the Mg-1 Gd and Mg-5 Gd alloys as matrix grains, whereas in the Mg-10 Gd case they are mostly extension twins.

The activation of twinning in magnesium alloys is also influenced by the grain size. For example, Wei Rong et al. [37] found that Mg-Gd-Zn-Zr alloys with a bimodal structure have better tensile-compressive symmetry than alloys with a uniform microstructure. The grains with larger size are more conducive to twinning activation, resulting in more balanced slip and twinning behavior during tensile and compressive processes. In this study, all three alloys had average grain sizes larger than 5 μm after D-ECAP, therefore, twinning was not suppressed (it can be only suppressed below 3 μm [14,15]). Fig. 11 shows the microstructural morphology of these three alloys after tensile and compressive deformation. It is generally believed that under tension at room temperature, the twinning activity in Mg alloys is relatively low. The surface fraction of twins in tensile testing was estimated by identifying the length fraction of the twin boundaries with respect to all other boundaries. Fig. 12 shows with red lines the twin boundaries. Indeed, the twin activity was quite low in tension in the Mg—1Gd alloy, only 3.25 %. With the increase of Gd content, the activation of deformation twins increased; it was 4.68 % for the Mg-5 Gd alloy, and 15.73 % for the Mg-10 Gd sample.

During compression, the activation of extension twins is expected to be higher than in tension. However, when the twin density becomes very high (above 50 %), it is hard to distinguish between the mother grains and the twins. To overcome this difficulty, a method has been proposed by Sahoo et al. [64]. This method is based on the All Twin Variant (ATV) polycrystal modeling and was confirmed by experimental results in compression of Mg. It has been proved that a partition between mother grains and twins can be done using the Schmid factors of the prismatic slip systems. Namely, if all Schmid factors of prismatic slip in a grain are relatively low, then this grain is highly probably a twin. We employed this approach in the present investigation. Fig. 13a-c presents the average Schmid factor distribution of prismatic slip after the compression tests. The regions with Schmidt factor less than 0.3 were considered to be twins, so the remaining surface fractions for mother grains were: 8.83 %, 11.11 % and 22.60 % for the Mg—1Gd, Mg—5Gd and Mg—10Gd samples (colored regions in Fig. 13d-f). Therefore, after compression, the area fraction of twinned areas increased significantly compared with tension case: up to 91.17 %, 88.89 % and 77.40 %.

4.2. Crystallographic texture

Generally, RE element addition and shear deformation produce relatively weak textures in Mg alloys. It is especially the case in the present D-ECAP process, because the direction of the deformation is inverted in the sample during its crossing into the second die, so the previously rotated grains were rotating in opposite directions, going back towards the initial texture, which was random in the initial state. Therefore, relatively weak textures were expected; indeed, the texture indices were relatively low; 2.93, 1.68 and 2.35 in the 1 %, 5 %, and 10

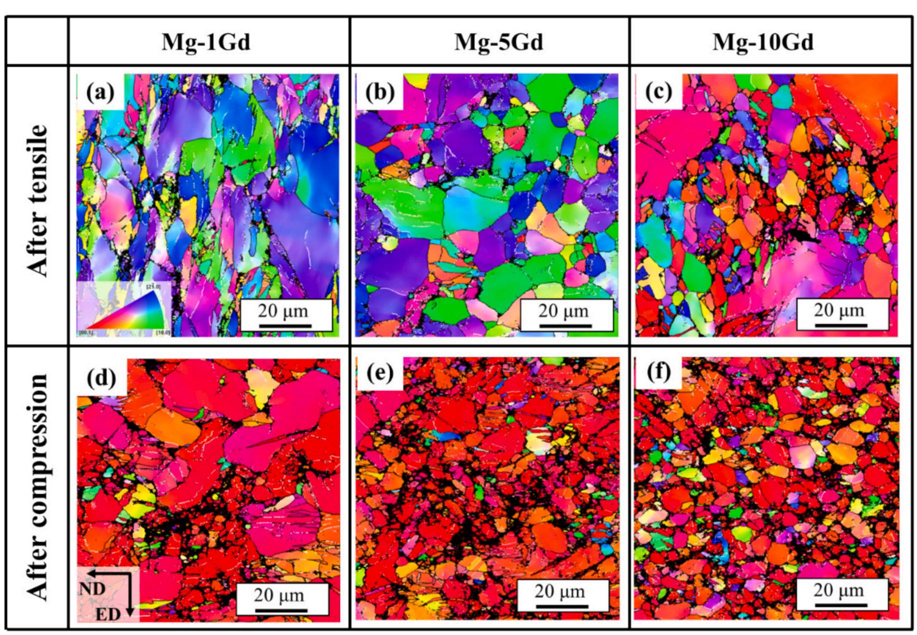

Fig. 11. EBSD results of fractured samples after tensile or compression test: (a,d) Mg-1Gd; (b,e) Mg-5Gd; (c,f) Mg—10Gd, the low-angle grain boundaries (LAGBs; 2°-15°) are colored in white lines.

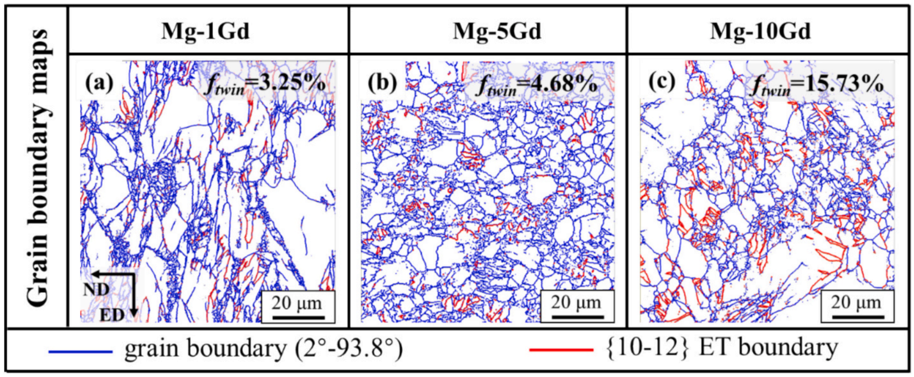

Fig. 12. Grain boundary maps of (a) Mg—1Gd, (b) Mg—5Gd and (c) Mg—10Gd samples after tensile tests.

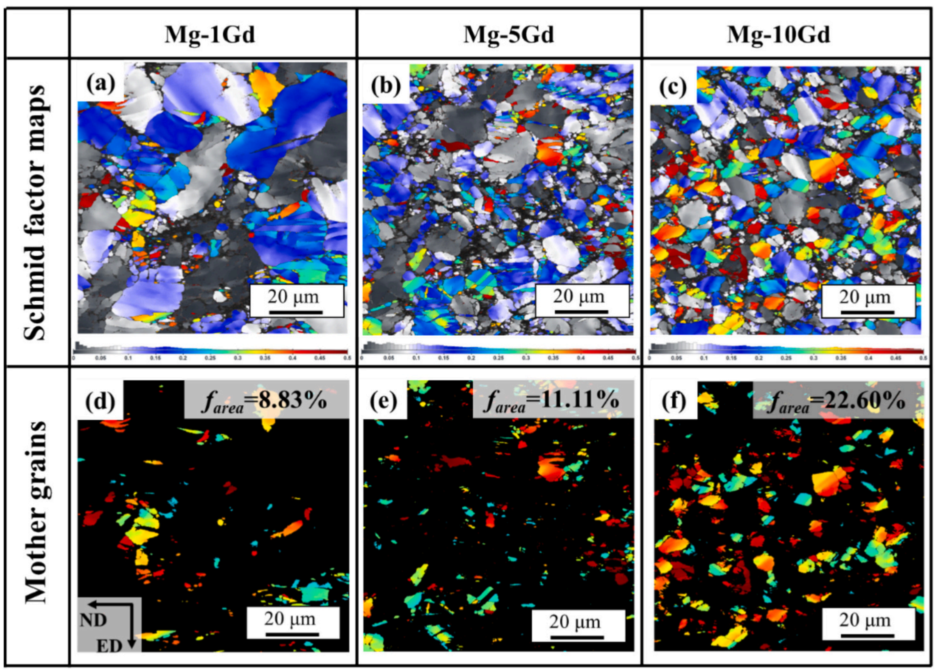

Fig. 13. (a-c): Schmid factor maps of primatic slip after compression; (d-f): regions with average Schmid factor of prismatic slip less than 0.3.

% Gd alloys, respectively.

As reported in [47], the C fiber texture is strongly characterized by <c + a > dislocation slip, however, B fiber texture is based on basal dislocation slip. In Mg—Gd alloy, both <c + a > dislocation slip and twins are commonly found [64]. During hot deformation processing in Mg—Gd alloy, such as extrusion, abundant twins are firstly activated in the initial deformation stage which can even cover the entire original grains (Gd contents 0–2.5 wt%) [50], which is a confirmation of twinning activation as described in section 3.1. As reported in [47], the C fibers are mostly induced by <c + a > dislocation slip and twins based on <c > −axis deformation, which is the case of appearance of the C fiber texture in Mg—1Gd and Mg—5Gd. However, when the Gd content increases to 10 %, the occurrence of deformation twinning can be effectively suppressed [33]. Therefore, basal slip becomes the main deformation mechanism at early stage of D-ECAP process which introduces the B fiber.

4.3. Polycrystal simulation

In order to explore deeply the role of the crystallographic texture in the slip/twinning activity and in the compression-tension asymmetry, polycrystal plasticity simulations have been carried out. The relaxed constraints version of the Taylor viscoplastic polycrystal approach was selected for the modeling. The experimental textures were discretized to 5000 orientations which were selected by the ATEX software [65] from the measured textures for representing the polycrystal. The basal, prismatic, pyramidal <c + a > type A, and ⟨10−12⟩ extension twins were used for plastic deformation with relative strengths of 1:5:4:1 with respect to basal slip, respectively. The strain rate sensitivity parameter for the viscoplastic glide of dislocations was 1/8. The selection of these values was based on previous simulation results on textures in Mg [47,66]. The elastic deformation of the polycrystal was not considered in the modeling.

In the construction of the polycrystal modeling one has to consider the particular deformation mode produced by twinning. Namely, when an extension twin is activated in compression, it is producing an extension, nearly perpendicular to the compression axis. It is the same effect in tensile deformation, with opposite sign. In order to permit the accommodation of this additional twin-induced deformation between neighbor grains, the strain components perpendicular to the axis of tensile/compression deformation were relaxed in the grains, so the following velocity gradient tensor ($\underline{L}$) was imposed on the individual grains of the polycrystal:

$$\underline{\underline{L}} = \begin{pmatrix} \dot{\varepsilon} & 0 & 0 \\ 0 & rel. & 0 \\ 0 & 0 & rel. \end{pmatrix} \tag{1}$$

Here '*rel.*' means the relaxation of the component, and $\dot{\varepsilon}$ is the tension/compression strain rate, applied along the x axis. The x-axis is the same as the final extrusion direction after D-ECAP (the ED). Then the stress tensor $\underline{\underline{\sigma}}$ corresponding to the strain rate states in Eq. (1) has the form:

$$\underline{\underline{\sigma}} = \begin{pmatrix} \sigma_{xx} & \sigma_{xy} & \sigma_{zx} \\ \sigma_{yx} & 0 & \sigma_{yz} \\ \sigma_{zx} & \sigma_{zy} & 0 \end{pmatrix} \tag{2}$$

The tensors in Eqs. (1–2) are representing a mixed boundary value problem for the grain, which can be solved iteratively, and the slip rates in the slip systems as well as the twinning rates in twin deformation can be obtained, together with the unknown components of the stress and strain rate tensors. The twinning systems were activated by the same viscoplastic law as for the dislocation glide. The simulation consisted in doing a single step, without applying significant plastic strain (instead, the strain rate was applied), so the result corresponds to the initial yield state of the sample without further hardening. The results obtained for the three measured textures containing 1–5-10 % Gd, as well as for a random texture, are presented in Table 3.

As can be seen in Table 3, the experimental CTA values were fairly well reproduced by the simulation (compare the data to Table 2). For the Mg—10Gd composition, the agreement is perfect, while slightly overestimated for the Mg—1Gd and Mg—5Gd alloys. For simulation of the CTA for random texture, two cases were considered: one is including the basal, prismatic, pyramidal slip and extension twinning, the other one only considering the mentioned three slip families in theVPSC modeling. It is interesting to note that for a random texture, if the deformation twinning could be activated during tension and compression, the CTA value is not equal to 1.0. Actually, one would expect isotropic mechanical behavior for a random texture, while the simulation informs us clearly an anisotropic response. The reason for this is the asymmetry in the slip/twin activities. When twinning is an available deformation mechanism for a Mg alloy with random texture distribution, the balanced activation of slip systems under tension and compression should be broken, especially for non-basal slip systems. This result indicates that the CTA in Mg alloys cannot be fully eliminated solely through randomization of the texture. For all simulation cases, twinning is much more active in compression than in tension. The difference in twinning involves differences in the slip activities. The most affected is pyramidal slip showing the same asymmetries as twinning, however, in the opposite sense. Basal slip is always very active, irrespectively of the deformation mode and the texture. Prismatic slip has relatively small activity, and always 2–3 times less active in compression than in tension, even in the random texture. Note that all these differences between tension and compression activities disappear if twinning is excluded as deformation mechanism. Such simulation result is presented in Table 3 for the random case, showing a very high pyramidal slip activity. Indeed, it is only pyramidal slip which can 'replace' twinning, if twinning is not available.

A CTA value higher than 1.0 (1.4) was measured in a Mg—10Gd alloy after extrusion [67] having a basal texture with c-axis perpendicular to the tensile/compression axis. That particular result was explained by shear bands, not with the combined effect of twinning and crystallographic texture. It is possible that if a polycrystal plasticity simulation would be applied to the textures of that study, a different conclusion could be made. It will be shown in our future study dealing with the ideal textures of magnesium deformed by shear, that CTA values larger than 1.0 can be readily obtained for specific textures.

Table 3 also shows the $\dot{\varepsilon}_{22}$ and $\dot{\varepsilon}_{33}$ strain rate components, which are resulting average values from the polycrystal simulation, although they are initially unknown. For an axisymmetric deformation mode, they should be equal. This is perfectly true for the random textured sample, and the values are nearly equal for the Mg—10Gd alloy sample. However, for the Mg—1Gd and Mg—5Gd alloyed samples, the deformation is not axisymmetric; it is nearer to a plane strain deformation mode. This is certainly due to the shear-type texture that developed during D-ECAP, which is not axisymmetric. The shear was taking place in D-ECAP following an inclined plane and direction with respect to ED.

4.4. Texture controlled material strength

In Mg—Gd binary alloys, Gd produces excellent solid solution strengthening and second-phase strengthening effects [68]. Grain refinement was achieved by large strain induced grain fragmentation, and relatively weak texture was obtained due to the strain reversal during processing. Solid solution strengthening contribution in Mg—10Gd alloy by Gd is approximately 56.7 MPa higher than that in Mg—1Gd alloy based on the calculation in Ref. [69]. According to the Hall-Petch relationship, grain refinement also has a significant impact on alloy strength. During the D-ECAP deformation process, when the Gd element content increased from 1 wt% to 5 wt%, the average grain size of the alloy significantly decreased by more than twice, and the grain size distribution became quite uniform. Nevertheless, despite a further increase in Gd content up to 10 %, the average grain size remained nearly unchanged. This resulted in a smaller increase in yield strength when increasing the Gd content from 5 wt% to 10 wt%, compared to Mg—1Gd and Mg—5Gd.

Furthermore, the strength of Mg—Gd alloys is also greatly influenced by the size and distribution of second-phase particles. In traditional extrusion and rolling processed Mg—Gd alloys, inhomogeneous distribution of precipitates is typically associated with heterogeneous grain-size distribution. This effect can result in a reduction of ductility of the alloy during tensile deformation. However, simple shear deformation mode is beneficial for a more uniform refinement and distribution of the solidified material after melting. Therefore, using D-ECAP, a better homogeneity can be expected, because D-ECAP is imposing shear

Table 3
Polycrystal plasticity simulation results for slip/twinning relative activity and strain response in tension and compression of the D-ECAP deformed samples containing 1–5-10 % Gd, as well as a random textured sample. CTA: simulated compression-tension yield stress ratio.

Sample	CTA	Deform. Mode	$\dot{\varepsilon}_{11}$ $1/s$	$\dot{\varepsilon}_{22}$ $1/s$	$\dot{\varepsilon}_{33}$ $1/s$	Basal Slip %	Prism. Slip %	Pyram. Slip %	Extension twin %
1Gd	0.60	Tension	2.00	−1.54	−0.46	35.6	14.7	44.1	5.6
		Compr.	−2.00	2.14	−0.14	48.1	4.8	6.9	40.2
5Gd	0.74	Tension	2.00	−1.29	−0.71	38.0	14.3	35.8	11.9
		Compr.	−2.00	1.60	0.40	46.6	7.5	14.0	31.9
10Gd	0.85	Tension	2.00	−1.06	−0.94	38.3	12.1	30.6	19.0
		Compr.	−2.00	1.07	0.93	43.8	5.2	23.5	27.5
Random Texture	0.81	Tension	2.00	−1.00	−1.00	37.0	14.7	32.3	16.0
		Compr.	−2.00	1.00	1.00	45.2	6.7	19.6	28.5
Random (no twin)	1.0	Tension	2.00	−1.00	−1.00	36.0	17.3	46.7	0.0
		Compr.	−2.00	1.00	1.00	36.0	17.3	46.7	0.0

deformation. At the processing temperature of the alloys, Gd is in solid solution, so the distribution of the Gd atoms becomes more uniform due to the applied shear. Then, when the sample is cooled down to room temperature, a more even precipitation can take place, due to the homogeneous distribution of the Gd atoms. Consequently, even in the Mg—10Gd alloy, the second-phase particles exhibit an almost random distribution.

Route C ECAP processing is more favorable for weakening the texture of magnesium alloys when compared to other routes of ECAP in the first two passes of deformation due to its strain reversal effect [61,70]. For ECAP of wrought magnesium alloys, improved ductility can be achieved by weakening the basal texture, or by developing it in inclined position with respect to the loading axis. As shown in the Results Section, the distribution of {0002} basal textures of the alloys tend to conform to the ideal shear texture components during D-ECAP processing. Nevertheless, due to the influence of the Gd element content, Mg—1Gd, Mg—5Gd, and Mg—10Gd alloys show different intensities of the same simple shear texture component and can be tilted with respect to the ideal positions.

5. Conclusions

Three homogenized Mg—Gd binary alloy with Gd addition of 1 wt%, 5 wt% and 10 wt% were processed by using D-ECAP method at a strain level of 1.15 in this study. The microstructure and texture evolution were systematically characterized. Quasi-static tensile and compression tests were conducted to analyze the mechanical properties, and the yield asymmetry was examined experimentally as well as by polycrystal plasticity simulations. The main conclusions are as follows:

(1) The D-ECAP process is beneficial for grain refinement of Mg—Gd binary alloy. The grain sizes of the processed samples were 13.4 μm, 5.6 μm, and 5.1 μm for the Gd contents of 1 wt%, 5 wt% and 10 wt%, respectively. The precipitates showed a random distribution with an average size less than 2 μm. With increasing Gd addition, grain orientations moved to the tilted C1-C2, and B fibers of ideal shear textures.

(2) The tensile strength and elongation of the alloys were simultaneously improved after D-ECAP: the flow stress reached 233.7 MPa in tensile strength of the Mg—10Gd alloy with a good tensile ductility of 27.12 % and a CTA value of 0.85 in compression/tension yield stress ratio.

(3) Polycrystal plasticity simulations were developed for the first time to obtain the compression/tensile yield stress ratios (CTA) by simulation. The results were in good agreement with the experimental observations. Information was obtained also on the slip and twinning activities from the simulations, confirming the experimental observations for twinning in tension/compression.

(4) One of the most interesting results of the polycrystal simulations was the anisotropy obtained for a random (isotropic) texture for the CTA value, which is 0.8; different from the expected CTA = 1.0 value.

CRediT authorship contribution statement

Dongsheng Han: Writing – original draft, Visualization, Methodology, Investigation. **Cai Chen:** Writing – review & editing, Supervision, Resources, Project administration, Funding acquisition, Formal analysis, Conceptualization. **Mingchuan Wang:** Visualization, Software, Investigation. **Nathalie Siredey-Schwaller:** Visualization, Investigation, Formal analysis. **Zhonghua Du:** Writing – review & editing, Validation, Supervision, Resources. **Sen Yang:** Validation, Supervision, Resources. **Fengjian Shi:** Resources, Investigation. **Benoit Beausir:** Validation, Software, Formal analysis. **Amèvi Tongne:** Validation, Software, Investigation. **Laszlo S. Toth:** Writing – review & editing, Validation, Supervision, Formal analysis, Conceptualization.

Declaration of competing interest

The authors declare that they have no known competing financial interests or personal relationships that could have appeared to influence the work reported in this paper.

Acknowledgements

The authors are grateful for the financial support provided by the National Natural Science Foundation of China (grant numbers 51901101). L.S. Toth was supported by the National Research, Development and Innovation Office, Hungary under K143800 “New avenues of production of bulk and composite nanostructured metals; experiments, characterization, modelling” project.

Data availability

Data will be made available on request.

References

[1] X. Chen, J. Zhang, M. Wang, W. Wang, D. Zhao, H. Huang, Q. Zhao, X. Xu, H. Zhang, G. Huang, Research progress of heterogeneous structure magnesium alloys: a review, J. Magnes. Alloys 12 (6) (2024) 2147–2181.
[2] S. Li, X. Li, C. Zhao, H. Liang, K. Liu, X. Du, W. Du, Recent progress of electrolytes for mg-air batteries: a review, J. Magnes. Alloys 12 (11) (2024) 4395–4421.
[3] M. Cheng, X. Liang, L. Cui, D. Guan, Y. Qu, J. Zhao, K. Guan, Magnesium-based nanocomposites for orthopedic applications: a review, J. Magnes. Alloys 12 (11) (2024) 4335–4362.
[4] J. Zhang, J. Miao, N. Balasubramani, D.H. Cho, T. Avey, C.Y. Chang, A.A. Luo, Magnesium research and applications: past, present and future, J. Magnes. Alloys 11 (11) (2023) 3867–3895.
[5] B. Shi, C. Yang, Y. Peng, F. Zhang, F. Pan, Anisotropy of wrought magnesium alloys: a focused overview, J. Magnes. Alloys 10 (6) (2022) 1476–1510.
[6] Z. Zhang, J. Yu, Y. Xue, B. Dong, X. Zhao, Q. Wang, Recent research and development on forming for large magnesium alloy components with high mechanical properties, J. Magnes. Alloys 11 (11) (2023) 4054–4081.
[8] Y. Xin, X. Zhou, Q. Liu, Suppressing the tension–compression yield asymmetry of mg alloy by hybrid extension twins structure, Mater. Sci. Eng. A 567 (2013) 9–13.
[9] L. Jingli, W. Di, H. Xiuzhu, W. Chen, C. Rongshi, X. Zhiyong, Tension-compression asymmetry of temperature dependencies in mg rare-earth alloys, J. Mater. Res. Technol. 27 (2023) 4929–4939.
[10] S. Lyu, R. Zheng, W. Xiao, Y. Huang, S. Gavras, N. Hort, G. Li, C. Ma, Abnormal extrusion texture and reversed yield asymmetry in a mg–Y-Sm-Zn-Zr alloy, Mater. Sci. Eng. A 760 (2019) 426–430.
[11] H.B. Chen, T.M. Liu, Y. Zhang, Y.B. Zhai, J.J. He, Reducing tension–compression yield asymmetry by free end torsion in extruded mg alloy, Mater. Sci. Technol. 32 (2) (2016) 111–118.
[12] J.-L. Ning, B. Xu, Y.-L. Feng, X.-D. Li, X.-K. Li, W.-P. Tong, Tension–compression yield asymmetry influenced by the variable deformation modes in gradient structure mg alloys, Acta Metall. Sinica (English Letters) 33 (2) (2019) 252–266.
[13] H. Su, Z. Chu, C. Xue, Y. Li, L. Ma, Effect of initial texture on the {10–12} twinning variants selection mechanism in AZ31 magnesium alloy, Mate. Res. Express 7 (8) (2020) 086503.
[14] A. Ghaderi, M.R. Barnett, Sensitivity of deformation twinning to grain size in titanium and magnesium, Acta Mater. 59 (20) (2011) 7824–7839.
[15] H. Fan, S. Aubry, A. Arsenlis, J.A. El-Awady, Grain size effects on dislocation and twinning mediated plasticity in magnesium, Scr. Mater. 112 (2016) 50–53.
[16] F. Han, X. Luo, Q. Liu, Z. Hou, K. Marthinsen, G.L. Wu, C. Hatzoglou, P. Kontis, X. Huang, The effect of grain size and rolling reduction on microstructure evolution and annealing hardening response of a mg-3Gd alloy, J. Magnes. Alloys (2023), https://doi.org/10.1016/j.jma.2023.09.025.
[17] S.W. Lee, S.H. Kim, W.K. Jo, W.H. Hong, W. Kim, B.G. Moon, S.H. Park, Twinning and slip behaviors and microstructural evolutions of extruded mg-1Gd alloy with rare-earth texture during tensile deformation, J. Alloys Compd. 791 (2019) 700–710.
[18] A. Imandoust, C.D. Barrett, H. El Kadiri, Effect of rare earth addition on {10$\bar{1}$2} twinning induced hardening in magnesium, Mater. Sci. Eng. A 720 (2018) 225–230.
[19] A. Gao, Q. Li, X. Chen, Z. Zheng, Twinning behavior in wrought magnesium alloys and its connection with texture, precipitates and mechanical properties, Trans. Indian Inst. Metals 77 (1) (2023) 17–31.
[20] S.M. Yin, C.H. Wang, Y.D. Diao, S.D. Wu, S.X. Li, Influence of grain size and texture on the yield asymmetry of mg-3Al-1Zn alloy, J. Mater. Sci. Technol. 27 (1) (2011) 29–34.
[21] X. Jiang, F. Shi, Q. Lu, J. Wang, J. Guo, T. Chen, Y. Guo, S. Chen, S. Lu, S. Wang, High strength and high ductility combination of biodegradable high-purity magnesium fabricated by forward extrusion and extrusion-shear process, J. Alloys Compd. 1026 (2025) 180388.

[22] Z. Zhang, J. Xie, J. Zhang, X.S. Yang, R. Wu, Towards designing high mechanical performance low-alloyed wrought magnesium alloys via grain boundary segregation strategy: a review, J. Magnes. Alloys 12 (5) (2024) 1774–1791.
[23] H. Wang, X.C. Luo, D.T. Zhang, C. Qiu, D.L. Chen, High-strength extruded magnesium alloys: a critical review, J. Mater. Sci. Technol. 199 (2024) 27–52.
[24] N. Su, Q. Wu, C. Ding, Y. Wu, L. Peng, Effect of Y and Gd solutes on grain refinement of the as-extruded mg-Gd(-Y)-Zn-Mn alloys, J. Alloys Compd. 968 (2023).
[25] J. Chen, J. Zhan, S. Kolawole, L. Tan, K. Yang, J. Wang, X. Su, Effects of different rare earth elements on the degradation and mechanical properties of the ECAP extruded mg alloys, Materials 15 (2) (2022).
[26] J. Luo, H. Yan, L.W. Lu, R.S. Chen, A.R. Wu, F.C. Yin, Cold rollability improvement by twinning and twin–slip synergy in an mg–Zn–Gd alloy with rare earth texture, J. Alloys Compd. 883 (2021) 160813.
[27] X.L. Hou, Y.X. Zhai, P. Zhang, S. Guo, Z.Z. Yuan, Q.F. Guan, Rare earth texture analysis of rectangular extruded mg alloys and a comparison of different alloying adding ways, Rare Metals 35 (11) (2016) 850–857.
[28] J.W. Lu, D.D. Yin, G.H. Huang, G.F. Quan, Y. Zeng, H. Zhou, Q.D. Wang, Plastic anisotropy and deformation behavior of extruded mg-Y sheets at elevated temperatures, Mater. Sci. Eng. A 700 (2017) 598–608.
[29] T. Al-Samman, Modification of texture and microstructure of magnesium alloy extrusions by particle-stimulated recrystallization, Mater. Sci. Eng. A 560 (2013) 561–566.
[30] M.M. Hoseini-Athar, R. Mahmudi, R.P. Babu, P. Hedström, Effect of Zn content on the microstructural stability and grain growth kinetics of fine-grained extruded mg–Gd–Zn alloys, J. Alloys Compd. 831 (2020) 154766.
[31] J. Zhang, S. Liu, R. Wu, L. Hou, M. Zhang, Recent developments in high-strength mg-RE-based alloys: focusing on mg-Gd and mg-Y systems, J. Magnes. Alloys 6 (3) (2018) 277–291.
[32] K. Máthis, A. Farkas, M. Knapek, A. Ostapovets, G. Farkas, G. Németh, P. Harcuba, D. Drozdenko, The influence of gadolinium concentration on the twin propagation rate in magnesium alloys, J. Alloys Compd. 948 (2023).
[33] C. He, Z. Li, D. Kong, X. Zhao, H. Chen, J.-F. Nie, Origin of profuse $\{11\bar{2}1\}$ deformation twins in Mg-Gd alloys, Scr. Mater. 191 (2021) 62–66.
[34] N. Stanford, M.R. Barnett, The origin of "rare earth" texture development in extruded mg-based alloys and its effect on tensile ductility, Mater. Sci. Eng. A 496 (1–2) (2008) 399–408.
[35] X. Hou, Z. Cao, L. Wang, S. Xu, S. Kamado, L. Wang, Microstructure and mechanical properties of extruded mg–8Gd–2Y–1Nd–0.3Zn–0.6Zr alloy, Mater. Sci. Eng. A 528 (25–26) (2011) 7805–7810.
[36] P. Hidalgo-Manrique, J.D. Robson, M.T. Pérez-Prado, Precipitation strengthening and reversed yield stress asymmetry in mg alloys containing rare-earth elements: a quantitative study, Acta Mater. 124 (2017) 456–467.
[37] W. Rong, Y. Zhang, Y. Wu, Y. Chen, M. Sun, J. Chen, L. Peng, The role of bimodal-grained structure in strengthening tensile strength and decreasing yield asymmetry of mg-Gd-Zn-Zr alloys, Mater. Sci. Eng. A 740-741 (2019) 262–273.
[38] J. Sun, B. Xu, Z. Yang, X. Zhuo, J. Han, Y. Wu, D. Song, H. Liu, J. Jiang, A. Ma, Developing an industrial-scale ECAP mg-Al-Zn alloy with multi-heterostructure for synchronously high strength and good ductility, Mater. Charact. 164 (2020) 110341.
[39] Y. Li, Y. Jiang, Q. Xu, A. Ma, J. Jiang, H. Liu, Y. Yuan, C. Qiu, Achieving single-pass high-reduction rolling and enhanced mechanical properties of AZ91 alloy by RD-ECAP pre-processing, Mater. Sci. Eng. A 804 (2021) 140717.
[40] C. Sun, H. Liu, C. Wang, J. Ju, G. Wang, J. Jiang, A. Ma, J. Bai, F. Xue, Y. Xin, Anisotropy investigation of an ECAP-processed mg-Al-ca-Mn alloy with synergistically enhanced mechanical properties and corrosion resistance, J. Alloys Compd. 911 (2022) 165046.
[41] Q. Zhang, Q. Li, X. Chen, Research progress of ultrafine grained magnesium alloy prepared by equal channel angular pressing, Mate. Res. Express 8 (2) (2021) 022001.
[42] L. Vuong, L. Jiang, J.J. Jonas, S. Godet, B. Verlinden, P. Van Houtte, Microstructure, texture and mechanical properties of AZ31 mg alloy produced by Equal Channel angular extrusion, Can. Metall. Q. 47 (4) (2013) 437–447.
[43] W.M. Gan, M.Y. Zheng, H. Chang, X.J. Wang, X.G. Qiao, K. Wu, B. Schwebke, H. G. Brokmeier, Microstructure and tensile property of the ECAPed pure magnesium, J. Alloys Compd. 470 (1–2) (2009) 256–262.
[44] L.B. Tong, M.Y. Zheng, X.S. Hu, K. Wu, S.W. Xu, S. Kamado, Y. Kojima, Influence of ECAP routes on microstructure and mechanical properties of mg–Zn–ca alloy, Mater. Sci. Eng. A 527 (16–17) (2010) 4250–4256.
[45] A.I. Alateyah, Effect of ECAP die angle and route type on the experimental evolution, crystallographic texture, and mechanical properties of pure magnesium, Open Eng. 13 (1) (2023).
[46] C. Chen, D. Han, M. Wang, T. Cai, N. Liang, B. Beausir, H. Liu, S. Yang, The effect of rotary-die Equal-Channel angular pressing process on the microstructure, the mechanical and friction properties of GW103 alloy, Materials 15 (24) (2022).
[47] B. Beausir, L.S. Tóth, K.W. Neale, Ideal orientations and persistence characteristics of hexagonal close packed crystals in simple shear, Acta Mater. 55 (8) (2007) 2695–2705.
[48] V.V. Stolyarov, Y.T. Zhu, I.V. Alexandrov, T.C. Lowe, R.Z. Valiev, Influence of ECAP routes on the microstructure and properties of pure Ti, Mat. Sci. Eng a-Struct 299 (1–2) (2001) 59–67.
[49] C. Chen, D. Han, M. Wang, S. Xu, T. Cai, S. Yang, F. Shi, B. Beausir, L.S. Toth, High strength and high ductility of mg-10Gd-3Y alloy achieved by a novel extrusion-shearing process, J. Alloys Compd. 931 (2023) 167498.
[50] J. Zhao, B. Jiang, J. Xu, W. He, G. Huang, F. Pan, The influence of Gd on the recrystallisation, texture and mechanical properties of mg alloy, Mater. Sci. Eng. A 839 (2022) 142867.
[51] M. Maghsoudi, H. Ovri, T. Krekeler, M. Ziehmer, E.T. Lilleodden, Effect of Gd solutes on the micromechanical response of twinning and detwinning in mg, Acta Mater. 258 (2023) 119202.
[52] D. Gu, J. Peng, S. Sun, F. Pan, On the solid solution substitutional position and properties of mg–Gd alloy, J. Mater. Res. Technol. 20 (2022) 2859–2871.
[53] G.M. Lee, S.H. Park, Underlying mechanisms of variation in yield asymmetry and strain hardening behavior of extruded pure mg with Gd addition, J. Magnes. Alloys 11 (6) (2023) 2165–2181.
[54] W. Fu, P. Dang, S. Guo, Z. Ren, D. Fang, X. Ding, J. Sun, Heterogeneous fiberous structured mg-Zn-Zr alloy with superior strength-ductility synergy, J. Mater. Sci. Technol. 134 (2023) 67–80.
[55] Q. Wang, H. Zhai, L. Wang, J. Xu, Y. Chen, B. Jiang, A new strong and ductile multicomponent rare-earth free mg–bi-based alloy achieved by extrusion and subsequent short-term annealing, Mater. Sci. Eng. A 860 (2022) 144309.
[56] X.Z. Han, W.C. Xu, D.B. Shan, Effect of precipitates on microstructures and properties of forged mg–10Gd–2Y–0.5Zn–0.3Zr alloy during ageing process, J. Alloys Compd. 509 (35) (2011) 8625–8631.
[57] J.K. Mason, C.A. Schuh, The generalized Mackenzie distribution: disorientation angle distributions for arbitrary textures, Acta Mater. 57 (14) (2009) 4186–4197.
[58] S. Sankaranarayanan, R.K. Sabat, S. Jayalakshmi, S. Suwas, M. Gupta, Effect of nanoscale boron carbide particle addition on the microstructural evolution and mechanical response of pure magnesium, Mater. Des. (1980–2015) 56 (2014) 428–436.
[59] L. Zhong, J. Peng, S. Sun, Y. Wang, Y. Lu, F. Pan, Microstructure and thermal conductivity of as-cast and as-solutionized mg–rare earth binary alloys, J. Mater. Sci. Technol. 33 (11) (2017) 1240–1248.
[60] I. Stulikova, B. Smola, J. Cizek, T. Kekule, O. Melikhova, H. Kudrnova, Natural and artificial aging in mg-Gd binary alloys, J. Alloys Compd. 738 (2018) 173–181.
[61] C.F. Gu, L.S. Tóth, The origin of strain reversal texture in equal channel angular pressing, Acta Mater. 59 (14) (2011) 5749–5757.
[62] Y. Liu, Y. Wei, Gradient driven anomalous reversible plasticity in conventional magnesium alloys, Extreme Mech. Lett. 9 (2016) 158–164.
[63] C. Tan, Q. Sun, G. Zhang, Y. Zhao, High-cycle fatigue of a titanium alloy: the role of microstructure in slip irreversibility and crack initiation, J. Mater. Sci. 55 (26) (2020) 12476–12487.
[64] S.K. Sahoo, S. Biswas, L.S. Toth, P.C. Gautam, B. Beausir, Strain hardening, twinning and texture evolution in magnesium alloy using the all twin variant polycrystal modelling approach, Int. J. Plast. 128 (2020).
[65] J.-J. Fundenberger, B. Beausir, Analysis Tools for electron and X-Ray Diffraction, ATEX-Software, www.atex-software.eu, Université de Lorraine - Metz, 2017.
[66] B. Beausir, S. Suwas, L.S. Tóth, K.W. Neale, J.-J. Fundenberger, Analysis of texture evolution in magnesium during equal channel angular extrusion, Acta Mater. 56 (2) (2008) 200–214.
[67] L. Yang, Q. Li, X. Chen, L. Yan, The microstructure evolution and abnormal yield asymmetry of extruded mg-10Gd-0.5Zr alloy, J. Mater. Res. Technol. 19 (2022) 4031–4043.
[68] M.H. Barezban, R. Roumina, H. Mirzadeh, R. Mahmudi, Effect of Gd on dynamic recrystallization behavior of magnesium during hot compression, Met. Mater. Int. 27 (5) (2019) 843–850.
[69] X. Li, W. Qi, K. Zheng, N. Zhou, Enhanced strength and ductility of mg–Gd–Y–Zr alloys by secondary extrusion, J. Magnes. Alloys 1 (1) (2013) 54–63.
[70] C.F. Gu, L.S. Tóth, C.H.J. Davies, Effect of strain reversal on texture and grain refinement in route C equal channel angular pressed copper, Scr. Mater. 65 (2) (2011) 167–170.

Further-reading

[7] X. Zhang, J. Li, Y. Shi, H. Yue, Q. Chen, Effect of pyramidal plane II twinning in tensile deformation on tensile–compression yield asymmetry in three orthogonal directions of mg alloy, J. Mater. Eng. Perform. 33 (2023) 8770–8777.